2018 International Conference on Unmanned Aircraft Systems (ICUAS)
Dallas, TX, USA, June 12-15, 2018

Ground Impact and Hazard Mitigation for Safer UAV Flight Response

Andrew Poissant, Lina Castano, and Huan Xu, *Member, IEEE*

***Abstract*— As Unmanned Aerial Vehicles (UAVs) become more commonplace, there is a growing need for safer flight control software that allows for the UAV to understand and autonomously react to various flight anomalies. Decision-making software must allow the aircraft to perform tasks such as detect and avoid, as well as respond to critical failures mid-flight. This paper develops a ground impact and hazard mitigation (GIHM) module that integrates the following: (1) consideration of flight failure modes, (2) generation of feasible ground impact footprints based on glide equations, (3) selection of safest response ground impact sites based on a high resolution LandScan USA population dataset, and (4) controlled descent to selected site. For a sample population distribution, integration of GIHM with standard UAV flight software shows a reduction of 20.396 casualties per 100,000 flight hours compared to the flight software without GIHM. A 96% reduction in fatalities per flight hour resulted from incorporating this module, which brings UAVs closer to being safe enough to be integrated into the National Airspace System (NAS).**

I. Introduction

Software for the control of Unmanned Aerial Vehicles (UAVs) has become increasingly sophisticated and elaborate over the past decade. The major focus on such software, however, has been on automatic control, not autonomous control [1]. Automatic control provides the necessary automation of nominal operational control, while autonomous control must allow for a level of autonomy that predicts and responds to any event and condition [1]. There is still a critical need for fully developed safety software within the UAV system architecture that can make informed decisions in the presence of flight anomalies [2].

Two major hazards associated with UAV operations are collisions between the UAV and a Conventionally-Piloted Aircraft (CPA), and impact of the UAV with terrain, people, or structures [3]. These hazards pose a large risk to the general public, with casualties being the worst-case scenario. UAVs can have accident rates as high as 32 accidents per 100,000 flight hours. This can be as high as 32 times higher than the accident rates for small general aviation aircraft, and 3,200 times higher than large airliners [2]. With UAV accident rates significantly higher than that of CPAs, there is a clear need for additional safety measures for UAV control software and hardware before they can be integrated into the National Airspace System (NAS).

This work was supported in part by the Maryland Industrial Partnerships (MIPS) Program and by Millennium Engineering and Integration, Co.

A. Poissant is with the Institute for Systems Research, University of Maryland, College Park, MD 20742 USA e-mail: apoissan@umd.edu.

L. Castano is with the Aerospace Engineering Department, University of Maryland, College Park, MD 20742 USA e-mail: linacs@umd.edu.

H. Xu is with the Aerospace Engineering Department and Institute for Systems Research, University of Maryland, College Park, MD 20742 USA e-mail: mumu@umd.edu.

A 2012 Congressional Research Service (CRS) Report detailed the required technology and standard procedures for safe UAV control software. The report requires UAVs to have technology and standard procedures for sensing and avoiding other air traffic under all possible scenarios, including loss of communications [4]. In addition to sensing and avoiding capabilities, the UAV must be able to autonomously return to base or determine a safe path to crash [4]. Furthermore, as detailed in [5], all UAVs must operate in restricted airspace or at extremely low altitudes. In order to integrate UAVs into the NAS, airborne safety must be ensured by avoiding midair collisions and guarding against ground impact. The focus of this paper is the development and integration of a module that guards against casualties due to ground impact.

A wide body of literature exists in assessing the collective risk UAVs pose, both in-air [6][7][2], and on the ground [6][7][8][9][10]. Ground risk models can be categorized into the following: failure mode, impact location, recovery, stress, exposure, incident stress, and harm [11]. Of these categories, the most relevant to our work are failure and impact location models.

Characterizing failure modes is an important aspect in guarding against ground impact because if a flight anomaly and the effect of that anomaly on the aircraft states are known, then the aircraft's reachable ground footprint can be calculated using gliding flight equations. The failure mode determines the capabilities and maneuverability of the aircraft, which must be considered when developing ground footprint models. For UAVs, these modes may include actuator failures, sensor failures, engine malfunction, loss of radio link and GPS, as well as structural damage such as a broken propeller, wing, etc., caused by unanticipated flight events [12]. Our paper focuses on two particular modes: engine malfunction and actuator failures.

Regarding impact location models, previous works have developed reachable ground footprints. [13] investigated the ability of a fixed-wing aircraft to glide to a designated emergency landing area. The authors in [3] and [14] use 6 degree-of-freedom models to develop ground impact models for determining the reachable ground envelope of UAVs, and [15] developed an emergency no-thrust flight trajectory plan. None of these works, however, incorporate flight control software into these models. They furthermore do not examine collective risk profiles that consider population data.

To understand the collective risk a UAV poses to a given area, accurate population data can be used. Previous work has used census data or local tax data [6][7][8][9][10]. However, such information can be hard to acquire and can be largely unrepresentative of the true population count for a given

978-1-5386-1353-5/18/$31.00 ©2018 IEEE

area. [16] used demographic population data for entire cities and states to generate population data for use in developing collective risk profiles. Using data at such large scales can result in great uncertainty when finer resolution population data is required. For this reason, LandScan USA data was used to obtain accurate population data. The LandScan USA dataset represents ambient population at 90 m resolution anywhere in the United States [17]. In previous literature, Landscan data has been used for mapping global impacts from climate change, building and evaluating population density models, mapping spread of dangerous diseases, and much more [18][19][20]. However, to our knowledge, LandScan data has never been used for the purpose of determining the lowest risk ground impact point for a UAV experiencing a hazardous flight anomaly.

Given the work described above, there is still a need for an all-encompassing ground impact mitigation system. The contribution of this paper lies in the integration of a novel ground impact and decision making model with a high resolution population dataset to provide high accuracy collective risk profiles for safer UAV response. Furthermore, this work integrates with a high-fidelity flight software that includes a mission plan, a path planning module, 6-DOF aircraft model, and flight controller. This integration of the reachable footprint and risk distribution profiles with the flight control software demonstrates the potential real-life implications of this work. Simulations provide a look into how UAVs react to these critical flight anomalies. For our mission configuration, we showed that with GIHM, fatalities per flight hour were decreased by 96%. The remainder of this paper is structured as follows: Section II describes the architecture and requirements of GIHM, Section III develops the feasible ground impact footprint models, Section IV details the fault modes and safest response, and Sections V and VI present a case study, discussion, and conclusions.

II. Context-Level Architecture and Requirements

A. Context-Level Architecture

Fig. 1 shows the system domain block definition diagram (BDD) for the ground impact and hazard mitigation (GIHM) module. The diagram provides a definition of the system and its environment in terms of the principal elements. GIHM is comprised of three sub-modules: fault mode detection, UAV ground impact, and safest response. The GIHM system interacts with its external systems, which consists of the UAV flight software, flight states, and the LandScan population dataset. The user initiates the flight by entering the mission plan in the form of waypoints and uploads the area of operation data from LandScan.

Fig. 2 details the system context BDD for GIHM. This BDD identifies how the system interacts with its user and external systems, its system boundaries, and state flows (data exchanged between blocks) between the system of interest, user, and external systems. The state flows for GIHM include the mission plan in the form of waypoints, UAV states sent to GIHM (GPS coordinates, airspeed, roll, pitch, and yaw),

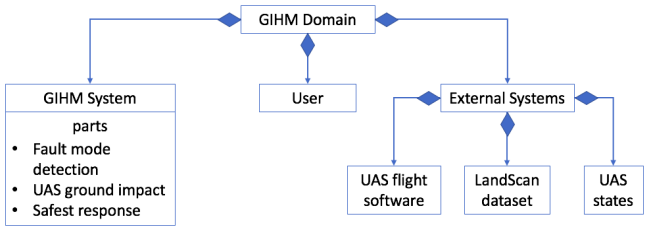

Fig. 1. GIHM system domain definition BDD. Establishes the domain of the system, which contains the GIHM system, user, and external systems.

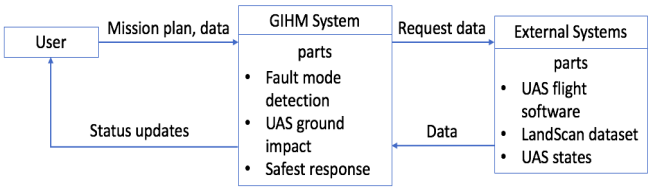

Fig. 2. GIHM system context BDD. Shows how the system interacts with its user and external systems.

and updated UAV states sent to the user. While GIHM was used fully autonomously in simulation (no input from the user after flight initiation), the level of autonomy can be adjusted to allow the user to be involved in the decision to use the new priority waypoints generated by GIHM. The system context BDD also shows that the UAV flight software sends data real-time to GIHM and GIHM determines if there is a critical flight anomaly with the goal of minimizing its ground impact. Before flight, the user selects from LandScan data the area of operation for the UAV and uploads that data for use in case of a flight anomaly. From this data, GIHM can send new waypoints to the UAV flight software, where the software executes the new mission plan.

B. System Requirements

Collective risk is the most commonly used metric in UAV ground models because it describes the aggregate risk to a population [3]. This metric has units of casualties per flight hour and shall be reduced comparing UAV flight control software with and without GIHM. GIHM is designed to reduce the number of casualties from UAV operations, and thus its collective risk. To accomplish this, the following system requirements need to be established where GIHM shall:

- Determine UAV flight states (e.g., GPS coordinates, airspeed, roll, pitch, yaw)
- Predict the feasible ground impact footprint (FGIF),
- Use the FGIF to extract local population count map from LandScan data,
- Process LandScan local population count map to extract lowest hazard zones as a candidate for landing,
- Select safest hazard response,
- Generate revised UAV flight plan to implement safest response.

When an anomaly is detected by the decision making module, GIHM must analyze the anomaly and determine which fault mode the aircraft is in. One approach is to detect

an anomaly by comparing current measured UAV states to expected ranges of vehicle states, e.g. airspeed, thrust, Euler angles, angular rates, system components and actuator deflections [21]. If any of the values are deemed to be out of their expected operating range, a corresponding fault mode is diagnosed. An inoperative engine will cause a decrease in thrust, causing the aircraft to deviate from its course and may pose a safety threat to nearby population in urban and suburban areas. For this work, the following two fault modes were considered:

1) Engine failure - UAV engine malfunction, resulting in no thrust.
2) Engine, rudder, and ailerons failure - UAV engine, rudder, and ailerons control surfaces failure. Ailerons and rudder control surfaces are stuck close to trim deflection.

With the states of the UAV known, and after detecting and diagnosing a flight anomaly, GIHM then predicts the FGIF using gliding flight equations and current UAV states. The local population data from LandScan is extracted, which is preloaded by the user before flight is initiated. Population data is then processed, with the lowest hazard zones being identified. With the lowest hazard landing areas known, GIHM selects the safest hazard response. The safest response consists of a new set of waypoints that the UAV follows to land or crash. This response is a function of the collective risk in the identified reachable zone and whether the starting or ending waypoints are within the FGIF. Finally, GIHM sends the new mission waypoints to the UAV flight control software for implementation. Because this work does not focus on landing site determination, the waypoint that GIHM provides can be considered a crash point.

C. GIHM Integration with UAV Flight Software

GIHM interfaces with a 6-DOF flight simulation software of a small, fixed-wing UAV, developed in Matlab/Simulink. Fig. 3 shows how GIHM interfaces with the flight simulation software. The UAV states are sent to GIHM, where GIHM determines whether the UAV is in a fault mode. In this work, a flight anomaly is detected when the UAV aircraft states are outside of a predetermined nominal range. If a fault mode is detected, GIHM sends back new mission GPS coordinates to the UAV flight control software. These new coordinates replace old mission waypoints.

The standard flight simulation architecture contains a path planning block, control system block, and aircraft block. The path planning block takes the initial 3D mission waypoints and calculates desired values so that the UAV can reach them. These values go into the autopilot which uses altitude and lateral-directional control for trajectory tracking via PID controllers. It then uses the desired navigation requirements to output actuator commands to the UAV. Finally, the aircraft block, which houses the UAV aircraft model, takes in actuator commands to update the new system states. The aircraft model uses aerodynamic forces and moments, and incorporates environmental factors related to altitude for air density and dynamic pressure calculations.

III. Feasible Ground Impact Footprint

The FGIF of an aircraft is the area on the ground where the UAV can reach. Due to the choice of simulating a prevailing engine failure, glider equations are used for the FGIF calculations. Fig. 4 depicts the FGIF concept and axis representation used in development of the FGIF models. Variables d_x and d_y represent displacements in the longitudinal and latitudinal direction, respectively, and d_z represents displacement in altitude. To calculate distance traveled in the x and y directions, gliding flight equations were used to model UAV flight performance. These equations were then iterated over an aircraft's 360° of maneuverability to obtain a full reachable envelope.

A. Gliding Flight

Calculation of the FGIF requires the vehicle's initial latitude, longitude, altitude, airspeed, roll angle, pitch angle, and yaw angle. These values are obtained from the UAV flight control software. The gliding flight equations are derived from the following equations of motion in the aircraft's longitudinal, lateral, and vertical axis respectively [13]:

$$m\frac{dv}{dt} = -mgsin(\theta) - D + Tcos(\theta), \tag{1}$$

$$mgcos(\theta)sin(\phi) = mv\dot{\psi}cos(\theta)cos(\phi), \tag{2}$$

$$mgcos(\theta)cos(\phi) - L - Tcos(\theta) = -mv\dot{\psi}cos(\theta)sin(\phi), \tag{3}$$

where ϕ, θ, and ψ are roll, pitch, and yaw angle, respectively. $\dot{\psi}$ is the turn rate of the aircraft, m is the aircraft's mass, g is acceleration of gravity, D is drag, and L is lift, and T is thrust. From here we make the following assumption: for an engine out case, we set T = 0, resulting in a constant speed and gliding flight. If a small glide angle approximation is used (which is the case for most aircraft), the gliding flight equations are simplified to:

$$0 = -mgsin(\theta) - D, \tag{4}$$

$$tan(\phi) = \frac{v\dot{\psi}}{g}, \tag{5}$$

$$mgcos(\phi) - L = -mv\dot{\psi}sin(\phi). \tag{6}$$

These are the three primary equations of motion for gliding flight in the aircraft's longitudinal, lateral, and vertical axis.

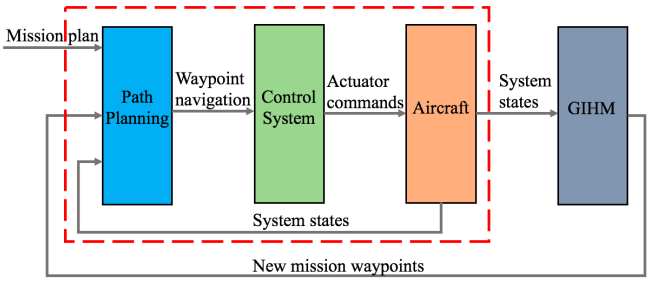

Fig. 3. GIHM integration with UAV flight software. The components inside the dashed red box contain the nominal UAV flight software architecture. GIHM takes the UAV system states as an input and outputs new mission waypoints if a flight anomaly is detected.

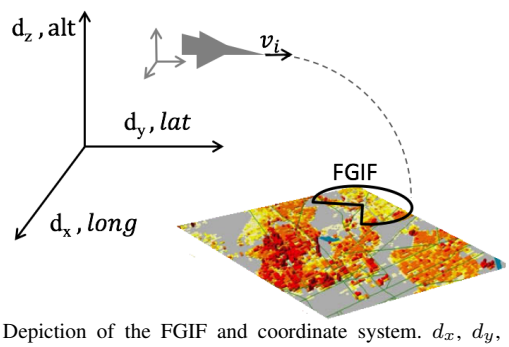

Fig. 4. Depiction of the FGIF and coordinate system. d_x, d_y, and d_z represent displacement in the longitude, latitude, and altitude directions, respectively. The UAV's reachable footprint is represented by the semi-circle labeled FGIF.

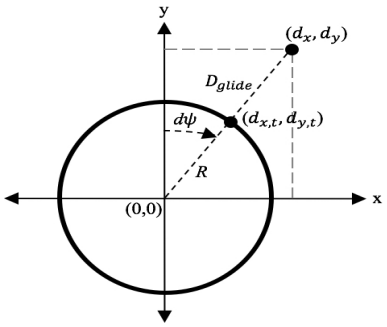

Fig. 5. Glide range derivation representation, which includes the turning phase and straight line phase.

B. Footprint Calculation

There are two phases to gliding flight: a turning phase and a straight line phase.

1) Turning phase: During a turn, an aircraft's airspeed will increase and height will decrease. To calculate the height loss during the turning phase, we use

$$\Delta h_{turn} = L_{arc}\frac{v_{s\phi}}{v_\phi}, \tag{7}$$

where $v_{s\phi}$ is the sink rate of the aircraft in the turning phase, v_ϕ is airspeed during the turning phase, and L_{arc} is the arc length of the circle made by the turn. v_ϕ and $v_{s\phi}$ are calculated using the following equations:

$$v_\phi = vsec^{\frac{1}{2}}(\phi), \tag{8}$$

$$v_{s\phi} = v_s sec^{\frac{3}{2}}(\phi). \tag{9}$$

L_{arc} is calculated using the following equations:

$$L_{arc} = Rd\psi, \tag{10}$$

$$R = \frac{v^2}{gtan(\phi)}, \tag{11}$$

where R is the radius of the circle and $d\psi$ is the total change in heading. $d\psi$ is bounded between $\pm\pi$ to account for an aircraft's ability to turn in the positive and negative directions.

An aircraft's rate of sink, v_s, is the amount of height loss per unit time the aircraft is flying during gliding flight. v_s is a function of the aircraft's drag, weight, and velocity through the following equation:

$$v_s = \frac{Dv}{W}. \tag{12}$$

To calculate drag, we can modify equations from [22], resulting in the following expression:

$$D = 0.5C_d\rho_0 v^2 S, \tag{13}$$

$$C_d = C_{do} + \frac{kC_L^2}{\pi A_r}, \tag{14}$$

where ρ_0 is the density of air at sea level, S is the wing area, C_{do} is the aircraft's profile drag, and k is the induced drag factor, determined by the aircraft wing dimensions, configuration, Reynolds Number and Mach Number. A_r is the aircraft's wing aspect ratio and C_L is the coefficient of lift.

To calculate C_L, it was assumed that the airfoil was cambered and had a thin airfoil. The following equation was used to calculate C_L, assuming a thin airfoil:

$$C_L = C_{Lo} + 2\pi\alpha, \tag{15}$$

where C_{Lo} is the aircraft's coefficient of lift at zero angle of attack and α is the aircraft's angle of attack. This equation is valid for small angle of attack and since the aircraft is not approaching stall conditions, the aircraft's angle of attack will be within the linear region of the angle of attack vs. coefficient of lift relationship.

Once the height loss during the turning phase is calculated, we next determine how far in the x and y directions the aircraft travels during the turning phase ($d_{x,t}$, $d_{y,t}$). Fig. 5 shows how $d_{x,t}$ and $d_{y,t}$ can be calculated based on simple geometric ideas. From this figure, we see that

$$d_{x,t} = Rsin(d\psi), \tag{16}$$

$$d_{y,t} = Rcos(d\psi). \tag{17}$$

With the total distance traveled during the turning phase known, the next phase is straight level flight.

2) Straight level phase: Distance traveled during straight level flight ($d_{x,s}$, $d_{y,s}$) is calculated using similar geometry to that of the turn phase:

$$d_{x,s} = D_{glide}sin(d\psi), \tag{18}$$

$$d_{y,s} = D_{glide}cos(d\psi). \tag{19}$$

Total ground distance traveled in the straight level flight, D_{glide} is calculated using the following equation:

$$D_{glide} = (h_i - \Delta h_{turn})\frac{v}{v_s}, \tag{20}$$

where h_i is the aircraft's initial height before entering gliding flight. The loss of height during a turn, Δh_{turn}, must not exceed the aircraft's initial height, which is an important condition when determining where the aircraft can maneuver to.

By adding total distances traveled during the turning and straight line phases, the total distance traveled in each direction can be calculated. This results in the final two

equations for distance traveled in the xy directions during gliding flight:

$$d_x = Rsin(d\psi) + D_{glide}sin(d\psi), \tag{21}$$

$$d_y = Rcos(d\psi) + D_{glide}cos(d\psi), \tag{22}$$

where d_x and d_y are the coordinates at the end of the glide, relative to the initial position and heading of the aircraft. The FGIF is simply comprised of all of the possible d_x and d_y combinations that the aircraft can reach. It is important to note that for this work it is assumed that there is no wind, which would otherwise have an effect on the gliding performance of a UAV.

Finally, it is important to consider whether an aircraft can actually execute the required turns when finalizing its FGIF. To account for the situation where the UAV reaches the ground during the turning phase, the following condition is required: if $\Delta h_{turn} > h_i$ then the aircraft cannot execute that turn, resulting in the corresponding d_x and d_y values being excluded in the FGIF.

IV. Fault Modes and Safest Response

A. Fault Modes

Now that models are established for gliding flight, we investigate the effects the two fault modes have on gliding performance. Faults are defined as unpermitted deviations of at least one characteristic property or parameter of the aircraft system from the acceptable or standard condition [21]. The impact of a fault can be small but it could also lead to overall system failure. After failure detection, a safe autonomous system needs to be able to classify the fault into an appropriate category in order to mitigate its effects. Faults are classified according to where they occur in the system, i.e. sensors, actuators and other components. Faults can also be classified as abrupt, incipient, or intermittent, with respect to their time characteristics.

In this work, we have considered an abrupt power system fault and a combined abrupt power system/actuator fault. The actuator fault implemented in simulation consists of aileron and rudder surfaces that got stuck close to trim value after a servo failure and remain at the deflections they had at the time of the fault [12]. It was assumed in this work that the UAV maintains some level of controllability when experiencing these faults.

1) Fault Mode 1, Engine Failure: In this fault mode, it is assumed that the UAV cannot accelerate but can change its heading and pitch angle. Because of this, the d_x and d_y equations derived above are used in their entirety to calculate the FGIF.

2) Fault Mode 2, Engine, Rudder, and Ailerons Failure: In this fault mode, it is assumed that the UAV cannot accelerate or change its heading, but can pitch. When the ailerons and rudder are stuck near trim value, the UAV is unable to change its heading. If the aircraft does not have heading control, it cannot execute a turning phase. Because the UAV cannot change heading, $d\psi = 0$, which results in only straight level flight. From this, the following modified gliding flight equations must be used to reflect that only straight level gliding flight can be achieved:

$$d_x = D_{glide}sin(\frac{\pi}{2} - \psi), \tag{23}$$

$$d_y = D_{glide}cos(\frac{\pi}{2} - \psi), \tag{24}$$

$$D_{glide} = h_i\frac{v}{v_s}. \tag{25}$$

The D_{glide} term was modified to exclude the Δh_{turn} because the aircraft is unable to turn. Notice that in the equations for d_x and d_y the $d_{x,t}$ and $d_{y,t}$ terms were removed because the aircraft is not turning while experiencing this fault mode. This results in a straight line reachable footprint.

Fig. 6 shows the FGIF of an aircraft traveling due north, experiencing Fault Mode 1 at different heights. The aircraft's initial position when experiencing the fault mode is at the origin of the plots. It can be seen that as the initial height of the aircraft increases, so does the FGIF (represented by the light blue shaded area of each plot). This is because the aircraft is able to glide for a longer time, resulting in a larger footprint.

Fig. 7 shows the FGIF of an aircraft traveling due north, experiencing Fault Mode 1 at different roll angles. The roll angles are only for the turning phase of gliding flight. The aircraft's roll angle is assumed to be 0 during the straight level phase. At smaller roll angles, the aircraft cannot execute turns to larger yaw angles fast enough. As a result, the aircraft cannot reach those larger angles before landing. This is seen in Fig. 7a where the aircraft experiences the fault mode while at a small roll angle. Because of this small roll angle, the FGIF is only part of a circle. As the roll angle increases, the aircraft can more quickly maneuver to larger yaw angles. This is seen in Fig. 7b and Fig. 7c where the aircraft has a larger roll angle and can reach the entire $\pm\pi$ range of yaw angles.

The FGIF of an aircraft experiencing the engine, rudder, and ailerons failure fault mode would simply be a line. Because there is no turning phase for this fault mode, the UAV cannot change its heading and therefore would only be able to fly at its current heading. However, the aircraft can still change its angle of attack using its elevator, which allows a straight-line footprint to be made, rather than an area.

B. Safest Response

With a model developed for the FGIF, we next develop a procedure for choosing the safest response. A searching algorithm was developed, which used the FGIF and UAV's current position to parse the LandScan USA data for the area in which the UAV could maneuver to. It then extracts the local minimum population value for which the UAV would pose the least collective risk. [N.B. The LandScan dataset is restricted for use by government agencies only. We use simulated data at this resolution to show how this dataset can be integrated.] The data structure of LandScan is a matrix whose rows and columns represent latitudinal and

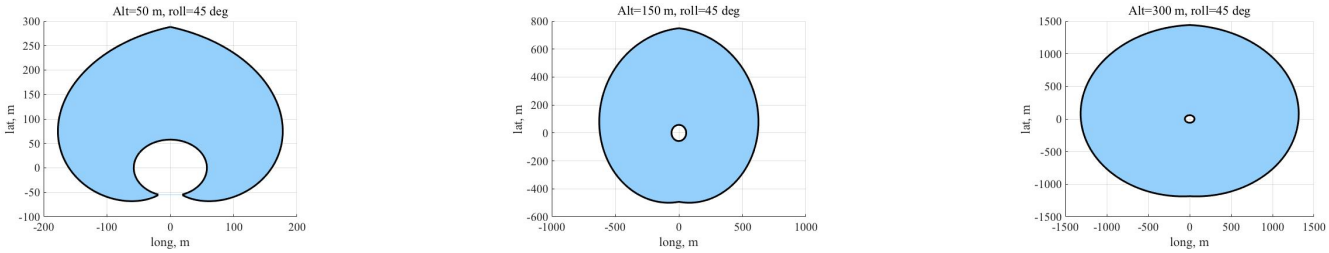

(a) (b) (c)

Fig. 6. Effect of aircraft height on FGIF for Fault Mode 1: (a) Alt=50 m, roll=45°. (b) Alt=150 m, roll=45°. (c) Alt=300 m, roll=45°. The light blue shaded area is the FGIF.

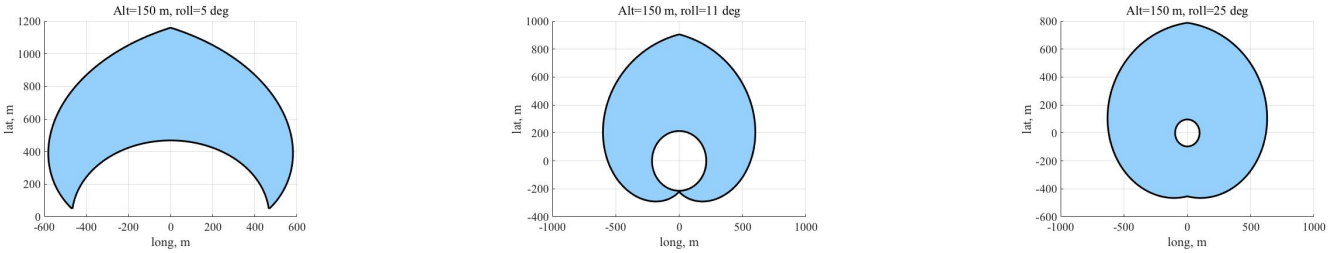

(a) (b) (c)

Fig. 7. Effect of aircraft roll angle on FGIF for Fault Mode 1: a) Alt=150 m, roll=5°. b) Alt=150 m, roll=11°. c) Alt=150 m, roll=25°. The light blue shaded area is the FGIF.

longitudinal coordinates. The value of each matrix cell is the population for that range of geodetic coordinates. LandScan USA data has some inherent uncertainty in its values, but the uncertainty is not addressed or quantified in the dataset's documentation.

Collective risk, also known as casualty expectation (CE), describes the aggregate risk that a UAV poses to a population of people. It is measured by expected number of casualties per flight hour [3]. Collective risk is calculated using the following equations [7]:

$$CE = PF \cdot PF \cdot PD \cdot AL \cdot PK \cdot S, \tag{26}$$

$$AL = (L + DG + DS + 2B) \cdot (W + 2B). \tag{27}$$

Definitions and the domain of variables for Eqns. 26 and 27 can be found in Table I. Probability of failure (PF) is expected number of mishaps per flight hour, population density (PD) is population count per square meter, probability of a fatality (PK) is the probability of a piece of the UAV striking a pedestrian and leading to a fatality, and shelter factor (S) is an estimate of how exposed a population is to falling vehicles or debris, with a factor of 0 and 1 representing completely sheltered and completely exposed, respectively. Lethal area (AL) is the area of which a fatality may occur when a vehicle or debris falls. Length (L) and width (W) refer to the wingspan and length of the aircraft, respectively, buffer (B) is a safety factor, glide distance (DG) is the distance traveled beginning when the UAV is at an altitude of 6 ft and ending when it reaches the ground, and distance to stop (DS) is the total distance from when the UAV reaches the ground to when it comes to a complete stop. Because it is assumed that the UAV will crash and not land, DS = 0.

Lethal area, length, width, glide distance, and distance to stop are all specific to the aircraft and aircraft dynamics.

TABLE I. Definitions of variables in casualty expectation equations.

Variable	Definition	Domain
CE	casualty expectation	[0, 6.43] fat/flt hr
PF	probability of failure	(0, 1]
PD	population density per square meter	[0, 0.022] pop/m^2
AL	lethal area	77.75 m^2*
PK	probability of fatality	[0, 1]
S	shelter factor	[0, 1]
L	length	1.83 m*
W	width	1.41 m*
B	buffer	1 ft
DG	glide distance at 6 ft altitude	8.02 m*
DS	distance to stop	0 m

*Starred terms do not have a range of values because they are highly specific to the aircraft's dynamics. Representative values were given for the UAV simulated in this work.

The upper range of population density is determined by the highest population density in the United States, located in Guttenberg, New York City. The resulting casualty expectation values can be as low as 0 fatalities per flight hour and as high as 6.43 fatalities per flight hour. For large airliners, the average casualty expectation is 0.01 fatalities per 100,000 flight hours and that of small general aviation aircraft is 0.1 fatalities per 100,000 flight hours [2]. However, the casualty expectation will be much higher than these values for UAVs because casualty expectation is proportional to probability of failure, and manned aircraft have very small probabilities of failure, approximately 0.000064%, compared to unmanned aircraft, approximately 2.17% [23][24]. This leads to a collective risk for small UAVs that is expected to be nearly 100,000 times larger than that of a manned aircraft.

For the purposes of this paper, probability of failure was assumed to be 0.0217, consistent with the maximum probability of failure for a small UAV defined by Sean

et al. [24]. The population density was found by dividing the population count from LandScan data by its respective area. The probability of fatality was found using methods explained by Range Safety Group, which was a function of the mass and speed of the aircraft [7]. A conservative shelter factor of 1 was used, representing a fully exposed population. Glide distance was calculated using the following equations [25]:

$$DG = tan(\frac{H_p}{\gamma}), \tag{28}$$

$$\gamma = tan^{-1}(\frac{H_p}{d}), \tag{29}$$

where γ is glide angle for this specific calculation, H_p is the height of an average person and d is the distance traveled from when the vehicle is at height H_p until when it hits the ground. This glide distance is different than glide distance derived in section III because this is the glide distance starting when the vehicle is at height H_p, not its mission plan height. By knowing the collective risk profile within the FGIF, the UAV is now able to find the point of local minimum risk and decide if the safest response is to fly to that minimum risk waypoint. Note that this model for CE does not account for uncertainties in population density, probability of failure, probability of fatality, etc. Uncertainty analysis is out of the scope of this work but would refine risk and fatality estimates.

While LandScan data is always available, it may not always be required in determining the safest response. If the mission endpoint is within the FGIF of the aircraft then the UAV should naturally land at that waypoint as its the safest response. Similarly, if the mission endpoint is not within the FGIF, but the mission start is, then the aircraft should fly back to where it started.

V. Case Study and Discussion

A. Problem Setup

In this case study, a small fixed-wing UAV was modeled. The aerodynamic characteristics used for the small UAV are seen in Table II.

TABLE II. Characteristics of the General Aviation UAV used in simulation.

Variable	Definition	Value
v	aircraft velocity	20 m/s
α_{max}	max angle of attack	6.25°
m	maximum take off weight	1.2 kg
L_w	wingspan	1.4 m
T_w	wing taper	1.95
AR	wing aspect ratio	6.4
w_c	wing aerodynamic chord	0.22 m
$airfoil$	wing airfoil	SD7037
C_{Li}, C_{Di}, C_{Mi}	Lift, Drag, Moment coeffs. derivs.	from airfoil

The UAV's nominal mission plan contains five waypoints and a home waypoint. The waypoints approach the University of Maryland, and a given fault mode is induced into the simulation 25, 45, 63, 80, 90, and 110 seconds into the simulation. These times were chosen to obtain a wide range of flight scenarios with the UAV at different points during its mission.

Model LandScan data was created in Matlab and was the same structure as LandScan USA data, but with a resolution of 30 m. The better resolution was required to show the utility of GIHM for small UAVs because of the size of the FGIF during simulations. Fixed blocks of higher population were created to mimic higher population expected in clusters of buildings at the University of Maryland. The dataset was preloaded into the UAV simulation and was parsed in real time when a fault mode was detected.

B. Results and Discussion

Table III summarizes the results of simulations for both fault modes at five fault mode times. By comparing the average casualty expectation with GIHM to the average casualty expectation without GIHM, we can conclude that the average casualty expectation is 20.396 fatalities per 100,000 flight hours lower with the GIHM module than without the module. For this mission configuration, this equates to an 96% decrease in fatalities per flight hour. Note that the units in Table III have units of fatalities per 100,000 flight hours, whereas CE has units of fatalities per flight hour in Table I. According to the FAA, a large airliner shall have a casualty expectation of 1 fatality per 1,000,000 flight hours, which is still far below the average casualty expectation value for the UAV with GIHM. This is because the probability of failure for this simulation is 2.17%, which is nearly one million times higher than the probability of failure for a large airliner (0.000064%).

TABLE III. Simulation results comparing CE with and without the GIHM module for both fault modes at six different fault times. CE has units of fatalities per 100,000 flight hours.

Fault Mode	Fault Time (s)	CE With GIHM	CE Without GIHM
1	25	0.000	9.690
2	25	1.124	8.471
1	45	0.024	13.350
2	45	2.709	11.670
1	63	0.017	61.650
2	63	1.124	53.900
1	80	0.017	15.760
2	80	3.698	13.780
1	95	0.017	19.400
2	95	4.509	16.960
1	110	0.000	18.140
2	110	1.157	15.860
Average		1.157	21.533

Nominal Flight: Fig. 8 and Fig. 9 show the flight simulation trajectory and altitude profile of the UAV under nominal operating conditions. The simulation terminates after the UAV reaches the fifth (final) waypoint. The plots of trajectory show the relative distance the UAV travels compared to the UAV's home waypoint. On all of the trajectory plots, the heat

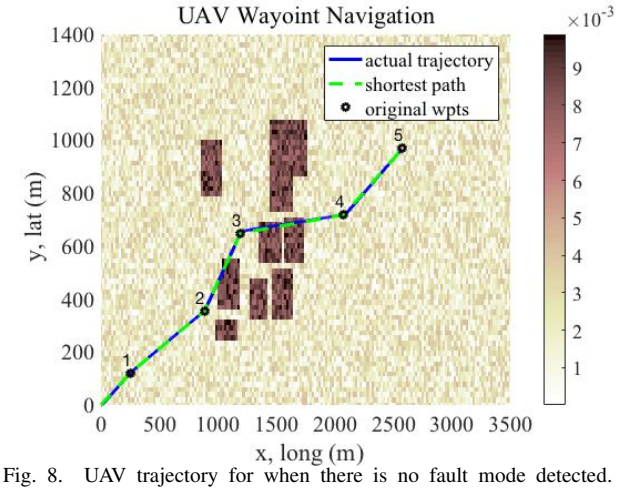

Fig. 8. UAV trajectory for when there is no fault mode detected. The aircraft starts from the home waypoint at the origin and travels to the waypoints in numerical order.

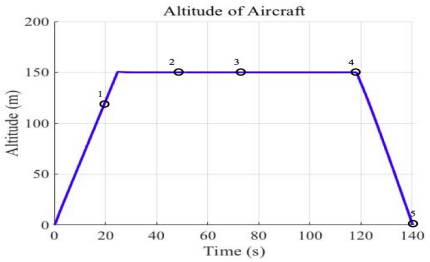

Fig. 9. UAV altitude plot as a function of time for when there is no fault mode detected. The numbered circles show the five mission waypoints. The UAV begins on the ground at the start, climbs to 150 m, then descends back to the ground when approaching waypoint 5.

map represents population count in that node with darker nodes representing highly populated areas. The population heat map is pixilated because the data was generated using randomized values. The randomized values were generated based on average population values in the University of Maryland area. When LandScan USA data is used, it can easily be integrated and the heat map of the population will be smoother and more accurate. It can be seen from the trajectory plot that the actual flight path of the UAV is very close to the shortest path, indicating an effective control scheme. Fig. 10 shows the Euler angle and Euler rate profiles for the nominal flight simulation. These will be used for comparison to the flight states of the UAV experiencing the two fault modes.

Fault Mode 1: Fig. 11 and Fig. 12 show the simulated flight trajectory and altitude profile of the UAV experiencing the engine out (Fault Mode 1) flight anomaly 80 s after mission plan initiation. At 80 s, as the UAV just passes waypoint 3, the engine out fault mode is detected, which results in the change of heading and change in mission plan. Fig. 12 also shows the throttle profile of the UAV experiencing Fault Mode 1 80 s after mission initiation. At 80 s, the throttle is at 0, which is consistent with the condition of the engine out case. From the altitude and trajectory plots, it can be concluded that the UAV found a minimum ground impact point and is flying to that point. The trajectory plot shows where the UAV would have landed compared to where it was able to maneuver. From the heat map, the new landing

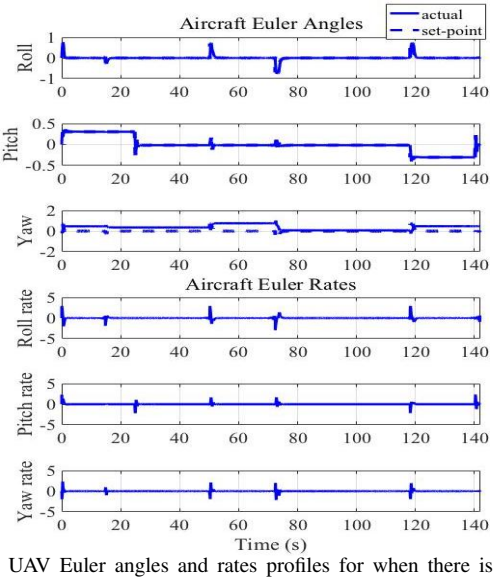

Fig. 10. UAV Euler angles and rates profiles for when there is no fault mode detected. Angles are in radians. The dashed line on the Euler angle plots show the controller commands and the solid line shows the actual aircraft states.

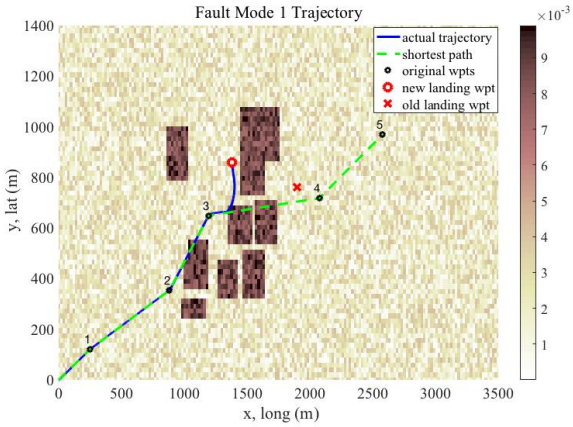

Fig. 11. UAV trajectory for when Fault Mode 1 is activated at 80 s. The aircraft starts from home at the origin and travels to the waypoints in numerical order until the fault mode is detected. New landing waypoint is the waypoint sent by GIHM and old landing waypoint is where the UAV would have landed without GIHM.

waypoint is in a less populated spot compared to the old landing point. A safety factor of 30 m was included so the UAV is not landing right next to the highly populated cluster of buildings. Fig. 13 shows the Euler angles and Euler rates for the UAV experiencing Fault Mode 1 80 s after flight initiation. Note the significant change in Euler angles and Euler rates at time 80 s, which is a result of the aircraft drastically changing heading to fly to the new priority waypoint generated by GIHM.

Fault Mode 2: Fig. 14 and Fig. 15 show the simulated flight trajectory and altitude profile of the UAV experiencing the engine, rudder, and ailerons failure (Fault Mode 2) flight anomaly 63 s after mission plan initiation. At 63 s, the UAV is almost at waypoint 3. At 63 s, the engine, rudder, and aileron failure fault mode is detected, which results in the change in mission plan. Fig. 15 also shows the throttle and rudder profiles of the UAV experiencing Fault Mode 2 63 s after mission initiation. It can be seen that at 63 s, throttle

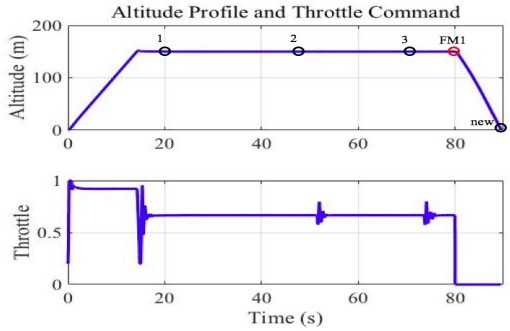

Fig. 12. UAV altitude and throttle command profiles for when Fault Mode 1 is activated at 80 s. The numbered circles show the mission waypoints, with the one labeled 'new' representing the new landing waypoint generated by GIHM. The red circle represents when the fault mode was detected. The aircraft starts on the ground, climbs to 150 m, then descends when the fault mode is detected at 80 s.

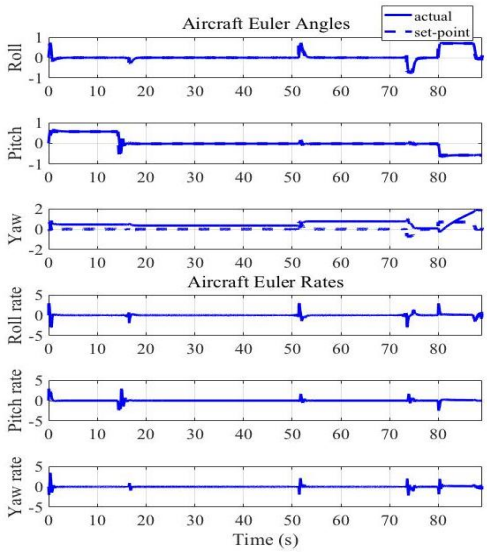

Fig. 13. UAV Euler angles and rates profiles for when Fault Mode 1 is activated at 80 s. Angles are in radians. The dashed line on the Euler angle plots show the controller commands and the solid line shows the actual aircraft states. The aircraft has drastic changes in all three Euler angles and rates when the fault mode is detected at 80 s because of the maneuvers made by the UAV to reach the safest landing point.

and rudder are 0, which is consistent with the condition of Fault Mode 2. From the altitude and trajectory plots, it can be concluded that the UAV found a minimum ground impact point and is flying to that point. The new priority waypoint is at the same heading as the UAV when the fault mode was detected because the UAV is unable to change its heading due to the rudder and aileron being inoperable. Fig. 14 shows where the UAV would have landed compared to where it was able to maneuver to. From the heat map, the UAV is able to change its pitch angle to guide the aircraft to the ground before it crashes in the highly populated group of buildings, which is where the UAV would have landed without GIHM.

Fig. 16 shows the Euler angles and Euler rates for the UAV experiencing Fault Mode 2 63 s after flight initiation. Note the significant change in Euler angles and Euler rates at time 80 s, which is a result of the aircraft drastically changing heading to fly to the new priority waypoint generated by GIHM. Notice that the roll and yaw angles remain unchanged after the fault mode is detected. This is because

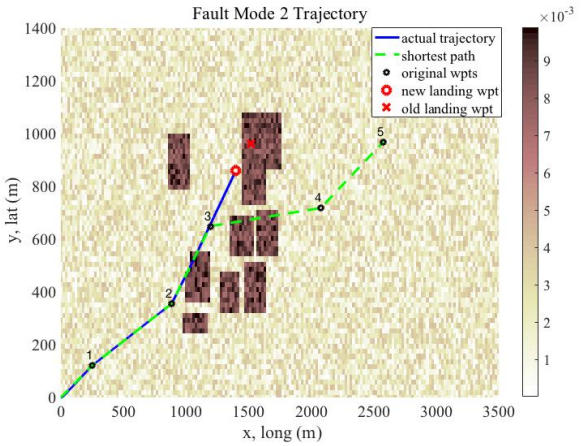

Fig. 14. UAV trajectory for when Fault Mode 2 is activated at 63 s. The aircraft starts from home at the origin and travels to the waypoints in numerical order until the fault mode is detected. New landing waypoint is the waypoint sent by GIHM and old landing waypoint is where the UAV would have landed without GIHM.

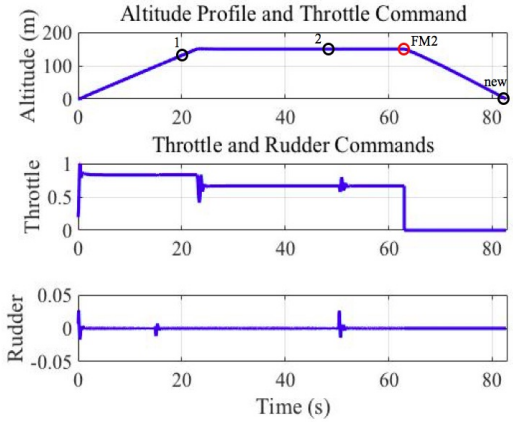

Fig. 15. UAV altitude, throttle, and rudder command profiles for when Fault Mode 2 is activated at 63 s. The numbered circles show the mission waypoints, with the one labeled 'new' representing the new landing waypoint generated by GIHM. The red circle represents when the fault mode was detected. The aircraft starts on the ground, climbs to 150 m, then descends when the fault mode is detected at 63 s.

the UAV cannot change its yaw or roll angles because of its malfunctioning rudder and ailerons.

Computation time for the GIHM module ranges between 0.01 s and 0.04 s on a 2015 MacBook Air with 1.6 GHz I5 processor, depending on which fault mode the UAV is in. Fault modes that allow for yaw and roll require more computation time because of the added amount of data points in the FGIF. From the plots, when the fault mode was detected, the UAV calculated the lowest casualty expectation landing waypoint and was able to maneuver to that point. The new landing points for all trajectory plots successfully avoided the highly populated areas, while the aircraft would have landed on the edge of the highly populated zones if the UAV had not used the GIHM module.

VI. Conclusion

Understanding the footprint for a UAV experiencing flight anomalies is an important first step in safer UAV control software. However, existing ground footprint models for UAV decision making either do not take into account population

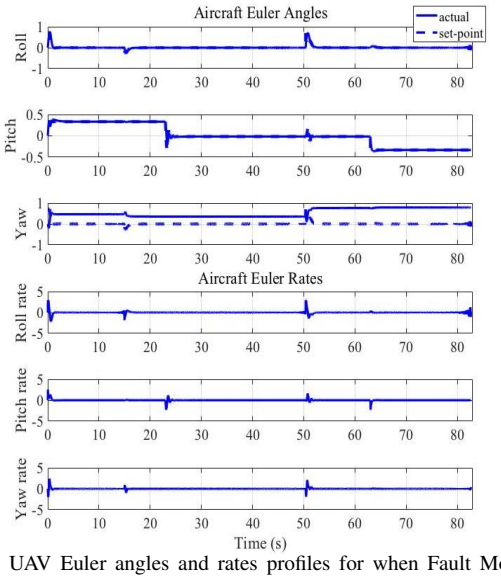

Fig. 16. UAV Euler angles and rates profiles for when Fault Mode 2 is activated at 63 s. Angles are in radians. The aircraft has drastic changes in pitch angle, but not roll or yaw angles when the fault mode is detected at 63 s because of the maneuvering limitations imposed by the fault mode.

density in the reachable footprint, or the population density data accuracy needs to be improved. The addition of a precise population dataset is an important addition to reachable ground footprint models because the UAV now possesses the ability to quantify its ground impact after determining where it can land.

This work combined a reachable ground footprint model with a precise spatial population dataset, all while integrating this work with a flight simulation software that included a 6-DOF aircraft model, path planning, and autopilot control. Our work successfully decreases the casualty expectation of a small UAV by an average of 20.396 fatalities per 100,000 flight hours, or a 96% decrease in casualty expectation. The development of the two fault modes allowed for a basis of investigation into where a UAV might land given the restrictions that specific fault modes cause and how the UAV can reduce casualty expectation for different flight anomalies.

Future work includes looking at uncertainty of system components, population density, and the environment, developing more engine out fault modes for other control surface malfunctions, developing fault modes for accelerated aircraft experiencing various control surface malfunctions, integrating a collision detection and avoidance module, addition of topology data for determining if a UAV has a sufficiently large landing site, and a more sophisticated decision making engine that allows the UAV to execute various flight control instability mitigation maneuvers during flight anomalies before diagnosing a fault mode.

ACKNOWLEDGMENT

The authors would like to thank Mike Briggs, Kerry Wisnosky, Ken Baird, and Adam Pederson from Millennium Engineering and Integration Company for their support and assistance in this work.

REFERENCES

[1] H. Chen, X. Wang, and Y. Li, "A survey on autonomous control for uav," in *International Conference on Artificial Intelligiance and Computational Intelligence*, 2009.

[2] R. Loh, Y. Bian, and T. Roe, "Uavs in civil airspace: safety requirements," *IEEE A&E Systems Magazine*, vol. 24, no. 1, pp. 5–17, 2009.

[3] P. Wu and R. Clothier, "The development of ground impact models for the analysis of the risks associated with unmanned aircraft operations over inhabited areas," in *Eleventh Probabilistic Safety Assessment and Management Conference*, June 2012.

[4] B. Elias, "Unmanned aircraft operations in the national airspace system," *Congressional Research Service Report for Congress*, 2012.

[5] K. Bhamidipati, D. Uhlig, and N. Neogi, "Engineering safety and reliability into uav systems: mitigating the ground impact hazard."

[6] C. Lum and B. Waggoner, "A risk based paradigm and model for unmanned aerial systems in the national airspace," in *American Institute of Aeronautics and Astonautics*, 2011.

[7] R. S. Group, "Range safety criteria for unmanned air vehicles."

[8] D. Burke, C. Hall, and S. Cook, "System-level airworthiness tool," in *Journal of Aircraft*, 2011, pp. 777–785.

[9] J. Stevenson, S. O'Young, and L. Rolland, "Estimated levels of safety for small unmanned aerial vehicles and risk mitigation strategies," in *Journal of Unmanned Vehicle Systems*, 2015, pp. 205–221.

[10] R. Clothier, R. Walker, N. Fulton, and D. Campbell, "A casualty risk analysis for unmanned aerial system (uas) operations over inhabited areas," in *Second Australasian Unmanned Air Vehicle Conference*, 2007, pp. 1–15.

[11] A. Washington, R. A. Clothier, and J. Silva, "A review of unmanned aircraft system ground risk models," *Progress in Aerospace Sciences*, 2017.

[12] C. M. Belcastro, D. H. Klyde, M. J. Logan, R. L. Newman, and J. V. Foster, "Experimental flight testing for assessing the safety of unmanned aircraft system safety-critical operations," in *17th AIAA Aviation Technology, Integration, and Operations Conference*, 2017, p. 3274.

[13] M. Coombes, W. Chen, and P. Render, "Reachability analysis of landing sites for forced landing of a uas," *International Conference on Unmanned Aircraft Systems (ICUS)*, 2013.

[14] N. Bradley and D. Burke, "Potential crash location (plc) model," in *Naval Air Warfare Center Aircraft Division*, 2012.

[15] E. Atkina, I. Portillo, and M. Strube, "Emergency flight planning applied to total loss of thurst," in *Journal of Aircraft*, 2006, pp. 1205–1216.

[16] L. Barr, R. Newman, E. Ancel, C. Belcastro, J. Foster, J. Evans, and D. Klyde, "Preliminary risk assessment for small unmanned aircraft systems," in *17th AIAA Aviation Technology, Integration, and Operations Conference*, 2017.

[17] B. Bhaduri, E. Bright, P. Coleman, and M. Urban, "Landscan usa: a high-resolution geospatial and temporal modeling approach for population distribution and dynamics," *GeoJournal*, vol. 69, pp. 103–117, 2007.

[18] X. Li, R. Rowley, J. Kostelnick, D. Braaten, J. Meisel, and K. Hulbutta, "Gis analysis of global impacts from sea level rise," *Photogrammetric Engineering and Remote Sensing*, vol. 75, no. 7, pp. 807–818, 2009.

[19] P. Sutton, C. Elvidge, and T. Obremski, "Building and evaluating models to estimate ambient population density," *Photogrammetric Engineering and Remote Sensing*, vol. 69, no. 5, pp. 545–553, 2003.

[20] C. Linard and A. Tatem, "Large-scale spatial population databases in infectious disease research," *International journal of health geographics*, 2012.

[21] M. Verhaegen, S. Kanev, R. Hallouzi, C. Jones, J. Maciejowski, and H. Smail, "Fault tolerant flight control-a survey," in *Fault tolerant flight control*. Springer, 2010, pp. 47–89.

[22] N. G. R. Center, *The Drag Coefficient*, accessed February 2, 2018. [Online]. Available: https://www.grc.nasa.gov/www/k-12/airplane/dragco.html

[23] Boeing, *Statistical Summary of Commercial Jet Airplane Accidents*, accessed September 1, 2017. [Online]. Available: http://www.boeing.com/resources/boeingdotcom/company/about_bca/pdf/statsum.pdfl

[24] S. Wolf, "Modeling small unmanned aerial system mishaps using logistic regression and artificial neural networks," 2012.

[25] NASA, *Glide angle and glide ratio*, accessed August 3, 2017. [Online]. Available: https://www.grc.nasa.gov/www/k-12/airplane/glidang.html